ICIC Express Letters
Part B: Applications
Volume **9**, Number **4**, April **2018**

ICIC International ©2018 ISSN 2185-2766
pp. **281–291**

RESEARCH ON TECHNOLOGY OF FLUID-IMPACT FATIGUE FRACTURE DEBURRING BASED ON INDUSTRIAL ROBOT

Haiyan Hu[1,2], Chunlin Tian[1], Jiandong Yang[2] and Hui Peng[1]

[1]College of Mechanical and Electric Engineering
Changchun University of Science and Technology
No. 7089, Weixing Road, Changchun 130022, P. R. China
1146682054@qq.com

[2]College of Engineering
Jilin Business and Technology College
No. 1666, Kalunhu Street, Changchun 130507, P. R. China
hhy1979_711@sina.com

Received October 2017; accepted January 2018

Abstract. *In this paper, a flexible machining system which combines fluid impact deburring technology and robot control technology is discussed. For the purpose of solving the problem caused by burrs in the horizontal hole, a method named fluid-impact fatigue fracture deburring is put forward in this paper in order to remove burrs. Firstly, a reasonable 3D model is established and then Fluent software is used to make a numerical simulation analysis on the internal flow field of brake cylinder and thus acquire the pressure distribution nephogram, velocity distribution nephogram and turbulence intensity nephogram for the inside of the pipe respectively, in addition to which the force on the burrs surrounded by hydraulic oil is calculated. Moreover, the first four orders of inherent frequency, vibration mode characteristics and stress frequency response diagram of burrs are obtained through further modal analysis and harmonic response analysis on such burrs. Finally, the resonance frequency of burrs can be calculated. Through comparative analysis on situation of burrs before and after deburring test, feasibility of this method is verified, which provides a reliable theoretical basis for removing burrs on automobile brake master cylinder.*

Keywords: Fluid-impact, Fatigue fracture, Deburring, Automobile brake master cylinder

1. **Introduction.** Brake master cylinder refers to the hydraulic actuator used to generate braking force in the braking system of a vehicle. Generally, the main hole of a master cylinder intersects with 4 to 5 cross-drilled holes and burrs may be generated at intersections during machining process [1]. Because of existence of a seal ring on the piston in the main hole, it is possible that such seal ring may be damaged by burrs (if any) and burrs may enter into the main hole under the effect of pressure oil and thus damage such seal ring or accelerate wear of seal ring, which will result in decrease of output pressure of pressure oil, change of its output performance curve and thus cause reduction of braking effect or even cause braking failure and serious traffic accidents [2]. Brake master cylinder is a key component concerning safety of a finished vehicle, which is directly related to personal safety of the driver and all passengers in a vehicle [3]. Therefore, research in this paper is of great significance in improving efficiency and quality of processing of brake master cylinder and reducing processing cost.

Fluid-impact fatigue fracture method refers to realizing fatigue fracture of the root of a burr under repeated alternating load generated by direction-changing and high-pressure fluid on such burr and then removal of such burr by the fluid [4]. An excessively small impact cannot ensure successful deburring, but an excessively large impact will require a more powerful high pressure generator and thus result in increased initial cost and cost

of use. Therefore, finite element analysis software should be used to conduct a numerical simulation analysis on internal passageway in the brake master cylinder and burrs, which provides a theoretical basis for research on deburring through fluid-impact fatigue fracture method. At present, there are many commonly used deburring methods. Comparison of various deburring methods is indicated in Table 1.

TABLE 1. Comparison of various deburring methods

Removal method	Applicable occasions	Abuse
Manual	Accuracy and efficiency requirements are not high	The waste rate is high and the labor intensity is high
Heat/high temperature	Higher surface accuracy	Large investment, there are safety problems and thermal stress problems
Electrolysis/ electrochemistry	The surface accuracy is high and the aperture is complex	Large investment, complex control, serious pollution
Ultrasonic	Complicated cavity deep hole	The removal rate is limited and the size of the workpiece is limited
Debris flow	Cross hole and miniaturization	Difficult to clean, difficult to achieve on-line monitoring
Fluid-impact Fatigue Fracture	Cross hole and miniaturization	Easy to clean, on-line monitoring can be achieved

By comparing the commonly used deburring methods in Table 1, the method used in this paper is more suitable for removing the burr of the automobile brake master cylinder.

2. **Robot System.** Stäubli six-axis industrial robot is used in this system. Compared with general robot arm, such robot arm has a more compact structure, for which the overall closed arm structure is adopted and all servo motors, wires, air pipes, etc., are arranged in the arm. Moreover, pressure in such arm is increased for the purpose of isolating electrical components from the external damp environment [5].

As for installation of robot, the top mounted installation method is adopted with sufficient consideration of the rotation angle of arm joints and mutual interference problem, for which working space should be maximized [6].

As for the control system, design of embedded PLC controller cabinet is adopted, in which SIEMENS S7-300 system expanded with digital and analog extended modules is used [7]. The system is connected to the HMI man-machine interface touch screen, robot controller, external data acquisition module, external computer, etc., as shown in Figure 1.

3. **Hydrodynamic Basis of Computation.** Hydraulic oil in an automotive brake master cylinder is viscous incompressible fluid, and the hydraulic fluid is turbulent fluid flow at the cross bore on a brake master cylinder, so the standard turbulence model k-ε is adopted to control the flow, for which the specific control equation is indicated as follows.

Theorem 3.1. *Mass Conservation Equation of Hydrodynamics*

An increase in the mass of a fluid element in unit time, is equal to the net mass of the element flowing into the body at the same time interval. According to this law, the mass conservation equation can be acquired:

$$\frac{\partial \rho}{\partial t} + \frac{\partial (\rho u)}{\partial x} + \frac{\partial (\rho v)}{\partial y} + \frac{\partial (\rho w)}{\partial z} = 0 \tag{1}$$

In this equation: ρ represents density (kg/m^3); t represents time; u, v, w represent velocity components in three directions x, y, z (m/s) [8].

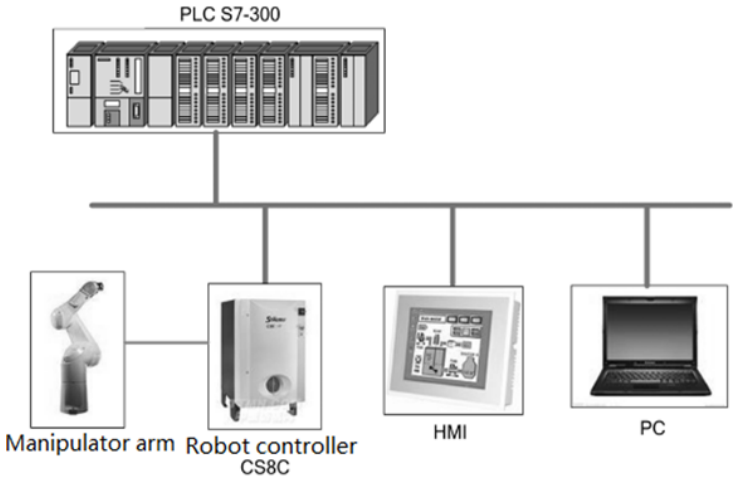

FIGURE 1. Control system diagram of robot

Theorem 3.2. *Momentum Conservation Equation of Hydrodynamics*

$$\begin{aligned}
&\frac{\partial(\rho u)}{\partial t}+\frac{\partial(\rho u u)}{\partial x}+\frac{\partial(\rho u v)}{\partial y}+\frac{\partial(\rho u w)}{\partial z}\\
&=\frac{\partial}{\partial x}\left(\mu\frac{\partial u}{\partial x}\right)+\frac{\partial}{\partial y}\left(\mu\frac{\partial u}{\partial y}\right)+\frac{\partial}{\partial z}\left(\mu\frac{\partial u}{\partial z}\right)-\frac{\partial p}{\partial x}+S_u\\
&\frac{\partial(\rho v)}{\partial t}+\frac{\partial(\rho v u)}{\partial x}+\frac{\partial(\rho v v)}{\partial y}+\frac{\partial(\rho v w)}{\partial z}\\
&=\frac{\partial}{\partial x}\left(\mu\frac{\partial v}{\partial x}\right)+\frac{\partial}{\partial y}\left(\mu\frac{\partial v}{\partial y}\right)+\frac{\partial}{\partial z}\left(\mu\frac{\partial v}{\partial z}\right)-\frac{\partial p}{\partial y}+S_v\\
&\frac{\partial(\rho w)}{\partial t}+\frac{\partial(\rho w u)}{\partial x}+\frac{\partial(\rho w v)}{\partial y}+\frac{\partial(\rho w w)}{\partial z}\\
&=\frac{\partial}{\partial x}\left(\mu\frac{\partial w}{\partial x}\right)+\frac{\partial}{\partial y}\left(\mu\frac{\partial w}{\partial y}\right)+\frac{\partial}{\partial z}\left(\mu\frac{\partial w}{\partial z}\right)-\frac{\partial p}{\partial z}+S_w
\end{aligned}\tag{2}$$

In this equation: ρ represents density; p represents instantaneous pressure; S_u, S_v, S_w represent generalized source terms; u, v, w represent average speeds; μ represents dynamic viscosity.

Theorem 3.3. *Standard k-ε Equation*

$$\mu_t=\rho c_u\frac{k^2}{\varepsilon}\tag{3}$$

In this equation: μ_t represents turbulent viscosity; c_u represents empirical constant (herein $c_u=0.09$); k represents turbulent kinetic energy; ε represents turbulent dissipation rate [8].

Theorem 3.4. *Transport equation of turbulent kinetic energy k*

$$\frac{\partial(\rho k)}{\partial t}+\frac{\partial(\rho k u_i)}{\partial x_i}=\frac{\partial}{\partial x_j}\left[\left(u+\frac{u_t}{\sigma_k}\right)\frac{\partial k}{\partial x_j}\right]+G_k-\rho\varepsilon\tag{4}$$

In this equation: G_k represents production item of turbulent kinetic energy k caused by mean velocity gradient, for which $G_k=u_t\left(\frac{\partial u_i}{\partial x_j}+\frac{\partial u_j}{\partial x_i}\right)\frac{\partial u_i}{\partial x_j}$; σ_k is empirical constant and $\sigma_k=1.0$ [9].

Theorem 3.5. *Transport equation of dissipation rate* ε

$$\frac{\partial(\rho\varepsilon)}{\partial t}+\frac{\partial(\rho\varepsilon u_i)}{\partial x_i}=\frac{\partial}{\partial x_j}\left[\left(u+\frac{u_t}{\sigma_\varepsilon}\right)\frac{\partial\varepsilon}{\partial x_j}\right]+\frac{C_{1\varepsilon}\varepsilon}{k}G_k-C_{2\varepsilon}\rho\frac{\varepsilon^2}{k} \tag{5}$$

In this equation: $C_{1\varepsilon}$ *is empirical constant;* $C_{1\varepsilon}=1.44$*;* $C_{2\varepsilon}=1.92$*;* $\sigma_\varepsilon=1.3$.

4. Analysis on Flow Field in Pipe of Automotive Brake Master Cylinder.

4.1. **Geometric modeling.** The three-dimensional model of the brake master cylinder of a certain type of automobile is as shown in Figure 2. The internal wall surface of the brake master cylinder is extracted by using *ANSYS* fluid analysis software, based on which fluid area can be generated.

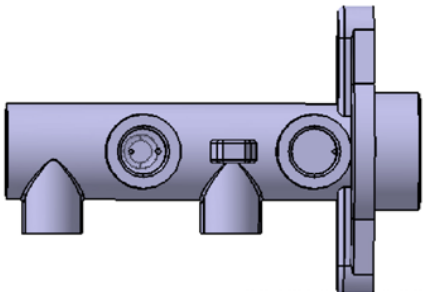

FIGURE 2. 3D model of automotive brake master cylinder

4.2. **Simplification of geometric model.** During numerical simulation analysis, the model should be firstly simplified to eliminate unconcerned features and improve speed and accuracy of computation [10]. Due to the fact that automotive brake master cylinder is complicated, a cross bore with burrs is selected to conduct simulation, for which the simplified model should be used for analysis.

4.3. **Mesh generation.** Mesh is spatial discretization of a geometric model, for which rationality of mesh generation can determine reliability of result of computation in a direct way [11]. In this paper, meshing software is used to conduct mesh generation for the above geometric model and the method of tetrahedral mesh generation is chosen to realize mesh generation, in addition to which an expanding layer is set at the wall surface. There are 90862 mesh cells and 31501 nodes in the mesh, and result of mesh generation is indicated in Figure 3.

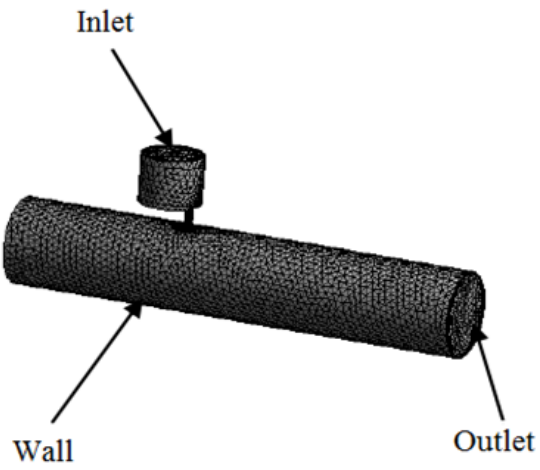

FIGURE 3. Mesh generation

4.4. **Setting of boundary conditions and relevant fluid parameters.** Boundary conditions for fluid computation area of the model include boundary conditions of pressure inlet, pressure outlet and solid wall surface [12]. Operating environment is under standard atmospheric pressure. The inlet pressure is 30Mpa and the outlet pressure is 0Mpa. Contact boundary between fluid and wall surface is non-slipping wall surface. Hydraulic oil herein used should be incompressible viscous fluid. Density and dynamic viscosity of hydraulic oil are set as 872kg/m^3 and 0.028kg/(m.s) respectively, based on which the phenomenon of no heat transfer in the pipe is computed without consideration of the gravity effect. Finite volume method is used to conduct numerical simulation of fluid channel and field inside the brake master cylinder, and standard k-ε turbulence model and *SIMPLE* algorithm are chosen to achieve numerical solution of the control equation.

5. Discussion and Analysis on Result of Numerical Simulation.

5.1. **Fluent analysis.** Fluent software is used to achieve solution for the model, for which the result is shown in Figure 4.

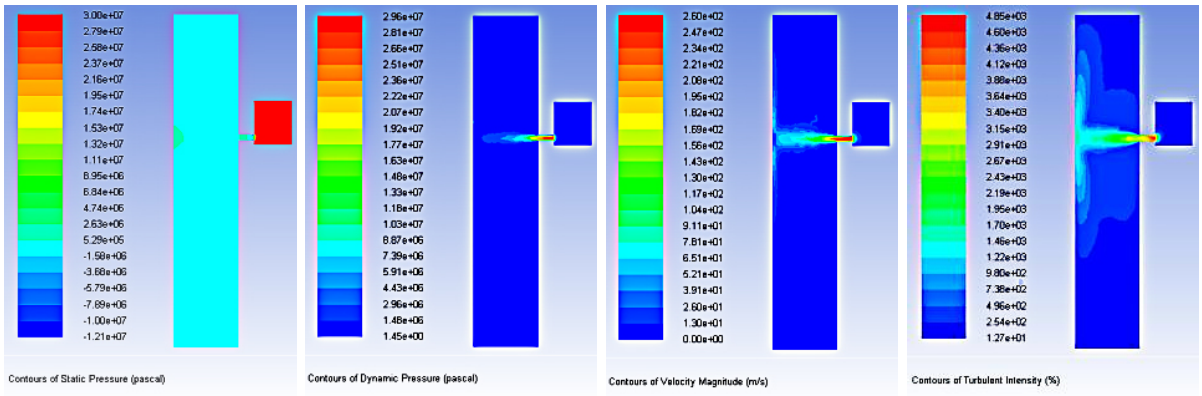

(a) Static pressure (b) Dynamic pressure (c) Velocity (d) Turbulence intensity

FIGURE 4. Numerical simulation analysis nephogram of flow field

Obviously, Figure 4(a) indicates that pressure has order-based progressive decrease in the brake master cylinder and outlet pressure is far less than inlet pressure, which meets the set boundary conditions. There is an obvious pressure difference at the intersecting bore of the brake master cylinder, which facilitates deburring.

Figure 4(b) indicates that as for the brake master cylinder, dynamic pressure at the inlet of cross bore is the largest, while dynamic pressure at the outlet is the smallest and dynamic pressure in the main bore decreases progressively. The larger the dynamic pressure is, the higher the ability of hydraulic oil in deburring with fluid impact-based fatigue fracture method in the area will be. It can be seen in the figure that at the intersection of main bore and cross bore on the brake master cylinder, pressure at the inlet is the largest because of the impact of turbulence. The maximum pressure around the burr is 2.07×10^7pa and pressure at the root of the burr is larger than pressure at the head, so it can be ensured that deburring can be realized in a better way.

Based on the velocity nephogram in Figure 4(c), when hydraulic oil enters into a relatively thin intersecting bore from the cross bore, speed of hydraulic oil increases suddenly, which facilitates removal of cross-bore burrs at the intersecting bore. It can be known based on the figure that the maximum speed appears at the intersection of the cross bore and the main bore on the brake master cylinder.

Based on the turbulence intensity nephogram in Figure 4(d), turbulence intensity at the cross bore of brake master cylinder is the largest and increase of turbulence intensity at the intersecting bore is obvious, for which activity of hydraulic oil at the intersecting

bore is instantaneously enhanced. Therefore, hydraulic oil at this segment has the most intense movement, which can ensure effective deburring.

5.2. **Modal analysis.** Burrs at the internal intersection are mainly uniform burrs with a height of 1-2mm and thickness of 0.1-0.2mm. A specific burr can be simplified as a cantilever and its cross section is a rectangle with a width of 0.2mm, a thickness of 0.1mm and a height of 1mm.

Material of the brake master cylinder material researched in this paper is cast aluminum alloy. As for its material properties, density of aluminum at room temperature should be $\rho = 2.7 \times 10^3 \text{kg/m}^3$; elastic modulus $\text{E} = 7.2 \times 10^4 \text{MPa}$, Poisson's ratio $\mu = 0.33$; tensile strength is within the range from 80 to 100MPa; yield strength is within the range from 100 to 170MPa and the fatigue limit strength is 32MPa.

For the purpose of making resonant frequency reach the inherent frequency under the effect of alternating load, model analysis on a burr is conducted. A burr should be imported into the model and a fixed constraint should be imposed at its left side, after which its inherent frequency and corresponding mode of vibration are calculated through *ANSYS Workbench* finite element simulation, based on which law of change is analyzed. Based on the actual working condition of the burr and subsequent requirements, the first four orders of modes are extracted for analysis in this paper. Modal frequency of the first four orders is indicated in Table 2.

TABLE 2. Modal frequency of the first 4 orders

Order	1	2	3	4
Frequency (Hz)	81983	1.59×10^5	4.91×10^5	5.87×10^5

It can be known based on the figure that the first-order and third-order modes show bending deflection of the burr at the direction of vertical width; the second-order mode shows bending deflection at the direction of vertical thickness, and the fourth-order mode shows first-order torsional deflection of the burr from the simulation results. Result of the above modal analysis lays a theoretical foundation for the following harmonic response analysis.

5.3. **Harmonic response analysis.** Harmonic response analysis, also known as frequency response analysis or frequency sweeping analysis, is used to determine steady-state response of a structure under the effect of a sinusoidal load with known frequency and amplitude [13]. Harmonic response analysis is often used to analyze structures under the influence of turbulence, for which the burr is analyzed through harmonic response analysis.

In *ANSYS Workbench*, harmonic response module and *Model* module should be connected. The force calculated by *Fluent* should be loaded on the burr (in the direction of Z) and magnitude of such force is $2.07 \times 10^7 \text{Pa}$, namely 4.14N. Frequency range, number of iterations and interval are set as 0-846000Hz, 300 times and 2820Hz respectively. Frequency response curves of stress in the directions of X, Y and Z on the upper surface are extracted to determine change of the burr. The results of the analysis are shown in Figure 5.

The following figure indicates that the largest stress amplitudes in the directions of X, Y and Z all appear at frequencies near 81780Hz, based on which it can be determined that obvious resonance occurs in the burr near 81780Hz. Stress frequency response in the direction of X is far larger than stress frequency responses in the directions of Y and Z, indicating that variation of stress mainly occurs in the direction of X. It can be known from result of modal analysis that first-order inherent frequency of the burr is 81983Hz,

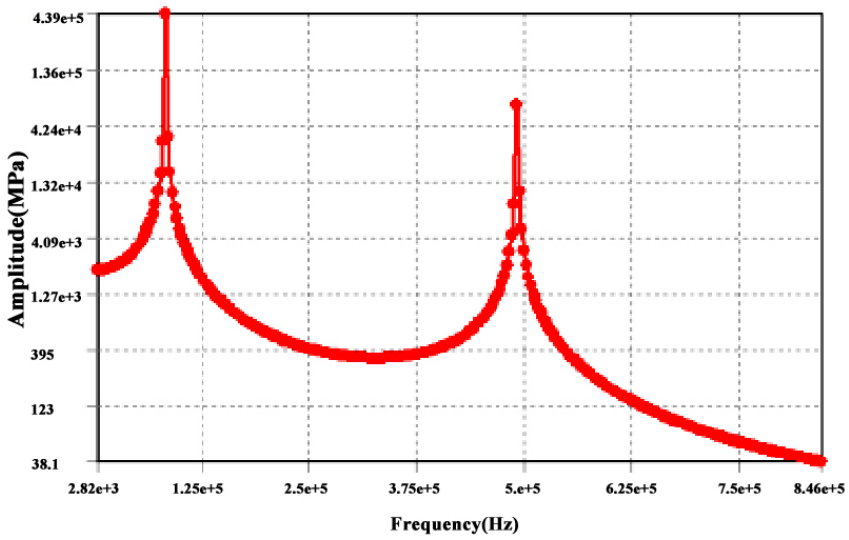

(a) Frequency response curves of stress in the directions of X

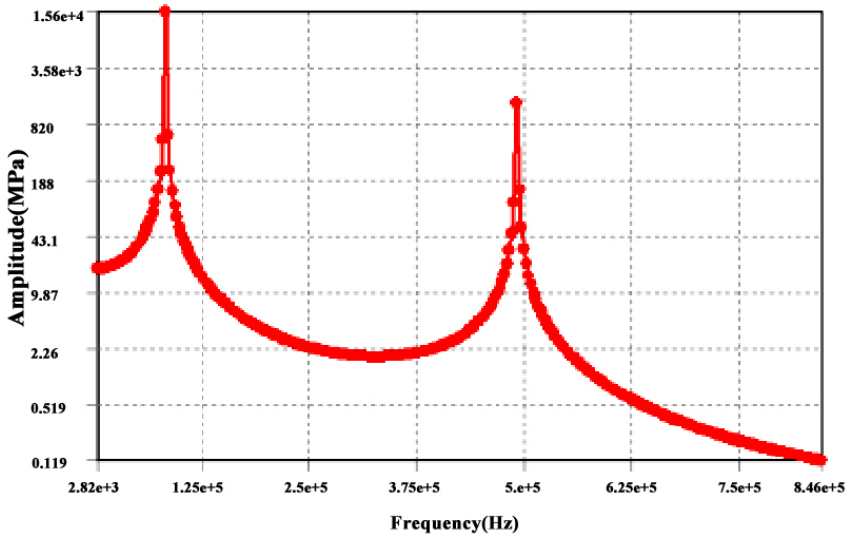

(b) Frequency response curves of stress in the directions of Y

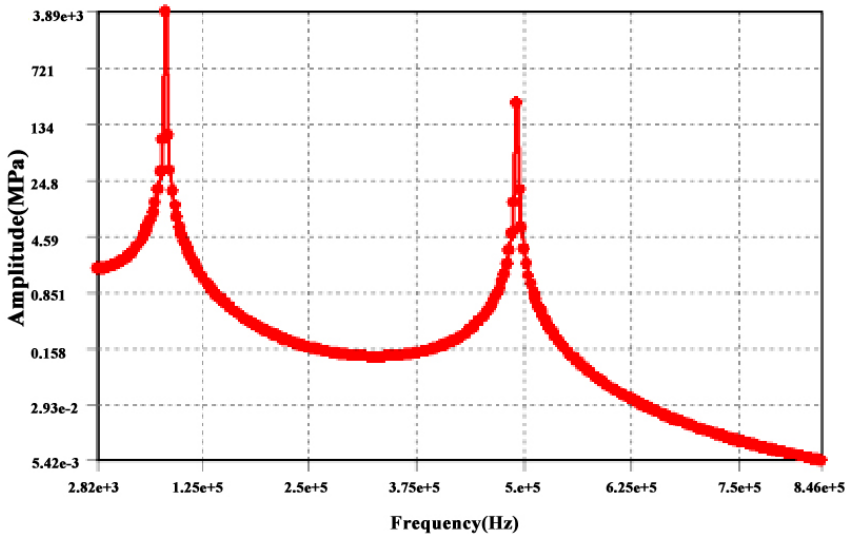

(c) Frequency response curves of stress in the directions of Z

FIGURE 5. Stress frequency response diagram

and resonance occurs in the burr easily when frequency reaches a point near 81780Hz. At this moment, change of the burr reaches the maximum degree.

The above figure indicates that vibration frequency of the burr stimulated under alternating load is 81780Hz. Situation of such burr at the frequency of 81780Hz is analyzed. When frequency reaches 81780Hz, displacement distribution of the entire burr indicates that the rightmost end of the burr has the largest displacement and the maximum value is 88.903mm, so free end of the burr will have bending fracture under the effect of an alternating load generated by 30MPa hydraulic oil. When frequency reaches 81780Hz, stress distribution of the entire burr indicates that external surface at the leftmost end of the burr sees the largest stress and the maximum value is 1.4459×10^6MPa. The minimum value in stress area of the small middle section is 43.712MPa, which is larger than the fatigue limit 32MPa of the burr of cast aluminum alloy. Therefore, the fixed end of the burr will have fatigue fracture under the alternating load generated by 30MPa hydraulic oil.

According to the above methods, the inlet pressure 10MPa, 5MPa, 1MPa are used in the simulation experiment, and get the relationship between inlet pressure and maximum/minimum stress in Table 3.

TABLE 3. The relationship between inlet pressure and maximum/minimum stress

Inlet pressure (MPa)	Maximum stress (MPa)	Minimum stress (MPa)
30	1.4459×10^6	43.712
10	6.3122×10^5	27.956
5	2.6968×10^5	11.377
1	6.3937×10^3	2.6721

Therefore, the fixed end of the burr will have fatigue fracture under the alternating load generated by 30MPa hydraulic oil.

6. **Experimental Analysis.** The samples were selected randomly, and the deburring experiment was carried out by the method proposed in this paper.

6.1. **Material and properties of the specimens (Table 4).**

TABLE 4. Material and properties of the samples

Material	Density	Elastic modulus	Poisson's ratio	Fatigue limit strength
Cast aluminum alloy (ZL107)	2.66×10^3kg/m^3	$E = 7.1 \times 10^5$MPa	0.32	32MPa

6.2. **Experimental result (Table 5, Table 6).** From the experimental data in Table 5, we can see that the simulation results are basically consistent with the experimental results, and the effect of deburring on the cross hole is better than that in the master cylinder.

From the experimental data in Table 6, we can see that the simulation results are basically consistent with the experimental results, and the best efficiency of deburring is 30MP.

Automobile brake master cylinder cross hole before and after deburring, respectively, cut and contrast analysis, is shown in Figure 6. Through the high power microscope observation, before deburring, you can see the obvious intersection hole burr exists, as shown in Figure 7(a). After deburring, you can see no burrs exist at the intersection, as shown in Figure 7(b).

TABLE 5. The relationship between location of Bur and machining result (Inlet pressure = 30MPa)

Width of Burr (mm) (Default height: 1mm)	Location of Bur	Machining Result
2mm	Inside the automotive brake master cylinder	The residual burr height < 0.5mm
	On the cross bore	The residual burr height < 0.1mm
1mm	Inside the automotive brake master cylinder	The residual burr height < 0.1mm
	On the cross bore	The residual burr height < 0.05mm

TABLE 6. The relationship between inlet pressure and machining result

Inlet pressure (MPa)	Location of Bur	Machining Result
30	Inside the automotive brake master cylinder	Basically clear
	On the cross bore	Completely clear
10	Inside the automotive brake master cylinder	No clear
	On the cross bore	Completely clear
5	Inside the automotive brake master cylinder	No clear
	On the cross bore	Completely clear
1	Inside the automotive brake master cylinder	No clear
	On the cross bore	Completely clear

FIGURE 6. Transverse incision of automobile brake master cylinder cross hole

7. **Conclusions.** Numerical simulation and experimental comparative analysis indicate that:

(1) Through analysis on numerical simulation nephograms of pressure, velocity, turbulence intensity inside the automotive brake master cylinder, it can be known that the burr on intersecting bore has the greatest ability in impact-based fatigue fracture.

(2) Through analysis on the first four orders of inherent frequency, characteristics of vibration mode and diagram of stress frequency response, resonant frequency of such burr is acquired. In addition, the minimum stress on the fixed end of the burr under the effect

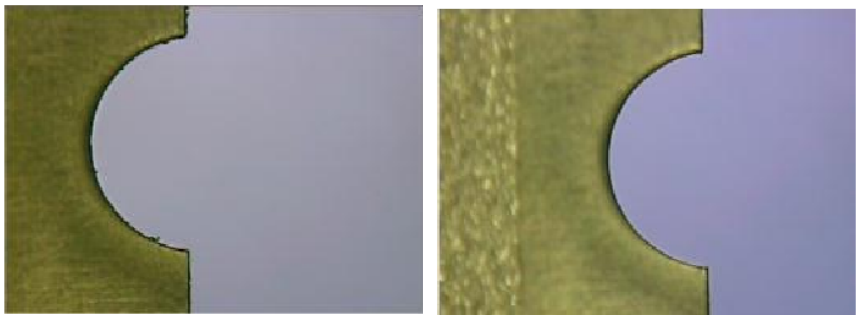

(a) Before removing the burr (b) After removing the burr

FIGURE 7. Before and after the burr contrast diagram

of resonant frequency is larger than fatigue limit of the burr, so the fixed end of such burr will have fatigue fracture under the alternating load of hydraulic oil.

(3) Based on the result of experimental comparative analysis, the deburring method based on fatigue fracture of burr caused by fluid impact is an effective deburring method, for which its efficiency is far greater than those traditional manual deburring methods.

Feasibility of the deburring method based on fluid impact-based fatigue fracture is verified through numerical simulation and experimental comparative analysis, which has a certain guiding significance for parameterization of fluid impact-based fatigue fracture method and provides a theoretical basis for optimal selection of parameters for deburring through fluid impact-based fatigue fracture method. In short, the development and application of the deburring robot based on the fluid impact fatigue fracture technology will provide a more versatile, flexible and efficient automated means for the deburring of parts. In the future, the optimization of the process parameters such as inlet pressure, hydraulic oil density and burr fracture model will be further studied.

Acknowledgment. The authors gratefully acknowledge the funding of this study by Science and Technology Development Plan of Jilin province (20120354) and Science and Technology Development Plan of Jilin province (20130204024GX) and Venture Fund Project for Personnel Studying Abroad of Jilin province (2010273) and Talent Development Project of Jilin province (20091328).

REFERENCES

[1] X. Zhang, The removal of tooling brake master cylinder cross burr: Anhui, *CN202824870U[P]*, 2013.
[2] J. Zhu, A shaft tool for horizontal hole deburring: Anhui, *CN104842013A[P]*, 2015.
[3] S. Liu, L. Guo and L. Hao, Design and research of automotive vacuum auxiliary braking system, *China Mechanical Engineering*, vol.26, no.13, pp.1840-1845, 2015 (in Chinese).
[4] N. Wang, *The High-Pressure Waterjet Deburring Research for Cross Hole of Chamber in the Given Workpiece*, Master Thesis, Changchun University of Science and Technology, Changchun, 2009 (in Chinese).
[5] W. Zhu, *Research on Key Technology of Inside-Out Punching Machine for Compensation Hole of Brake Pump Master Cylinder*, Hefei University of Technology, 2013 (in Chinese).
[6] Z. Xu, Present status of deburring processing for mechanical parts, *Machine Tool & Hydraulics*, vol.38, no.8, pp.111-113, 2010 (in Chinese).
[7] J. Liang, The development of robotic high pressure water deburring system, *Mechanical and Electrical Engineering Technology*, vol.41, no.7, pp.28-30, 2012 (in Chinese).
[8] H. K. Versteeg, *An Introduction to Computational Fluid Dynamics*, World Book Inc., 2010.
[9] H. Yan and D. Long, Research on modeling method for complex-structured mechanical components based on three-dimensional discrete element method, *ICIC Express Letters, Part B: Applications*, vol.8, no.3, pp.499-504, 2017.
[10] H. Yan and D. Long, 3D scanner-based corn seed modeling, *Applied Engineering in Agriculture*, vol.32, no.2, pp.181-188, 2016.

[11] B. C. Kwon, K. H. Kim, K. H. Kim and S. L. Ko, New abrasive deburring method using suction for micro burrs at intersecting holes, *CIRP Annals – Manufacturing Technology*, no.1, 2016.
[12] Z. Li, X. Li and X. Chen, The study on boundary conditions to the effect of mode analysis in FEA, *China Mechanical Engineering*, vol.19, no.9, pp.1083-1086, 2008 (in Chinese).
[13] X. Jia and B. Chen, Modal and Harmonic response analysis of large aspect ratio wing, *Science & Technology Vision*, pp.1-3, 2016.